World Academy of Science, Engineering and Technology
International Journal of Aerospace and Mechanical Engineering
Vol:8, No:12, 2014

A Study of Adaptive Fault Detection Method for GNSS Applications

Je Young Lee, Hee Sung Kim, Kwang Ho Choi, Joonhoo Lim, Sebum Chun, Hyung Keun Lee

***Abstract*—**This study is purposed to develop an efficient fault detection method for Global Navigation Satellite Systems (GNSS) applications based on adaptive noise covariance estimation. Due to the dependence on radio frequency signals, GNSS measurements are dominated by systematic errors in receiver's operating environment. In the proposed method, the pseudorange and carrier-phase measurement noise covariances are obtained at time propagations and measurement updates in process of Carrier-Smoothed Code (CSC) filtering, respectively. The test statistics for fault detection are generated by the estimated measurement noise covariances. To evaluate the fault detection capability, intentional faults were added to the filed-collected measurements. The experiment result shows that the proposed method is efficient in detecting unhealthy measurements and improves GNSS positioning accuracy against fault occurrences.

***Keywords*—**Adaptive estimation, fault detection, GNSS, residual.

I. Introduction

GLOBAL Navigation Satellite Systems (GNSS) have been applied to many positioning applications nowadays. The reliability of GNSS can be harmed due to many factors such as abnormal atmospheric conditions, malfunction of the receiver's software and hardware, and terrestrial objects illustrated in Fig. 1. Unhealthy measurements should be considered seriously especially in applying GNSS to aerospace or ground vehicles requiring high level of safety. One of the most popular approaches to deal with unhealthy measurements is to apply fault detection and isolation method to the measurements before generating position estimates. If fault detection function were not successful, undetected unhealthy measurements or parameters can drive the vehicle into dangerous situations. By the importance, fault detection methods have been studied actively by many researchers [1]-[3].

As widely known, the two most representative methods for GNSS fault detection are the parity method and the residual-based method [4], [5]. These methods are based on snap-shot measurement residuals obtained by the difference between the actual measurements and their estimates based on receiver position. However, the pre-computed position which facilitates the residual generation bears the possibility to be affected already by unhealthy measurements. This undesirable characteristic becomes more serious concern when two or more faults occur at the same time. To overcome this problem, the method utilizing projected pseudoranges is proposed [6]. This method checks abnormal trends in the variance of pseudorange and carrier phase measurement sequence based on the Carrier-Smoothed Code (CSC) principle [7].

This paper proposes efficient adaptive detection method for GNSS applications based on projected pseudoranges. The proposed method utilizes adaptive test statistics for fault detection based on estimated measurement noise covariances. The pseudorange and carrier-phase innovation sequences are obtained at time propagations and measurement updates in process of CSC filtering, respectively. The performance of the proposed method was evaluated by a field experiment.

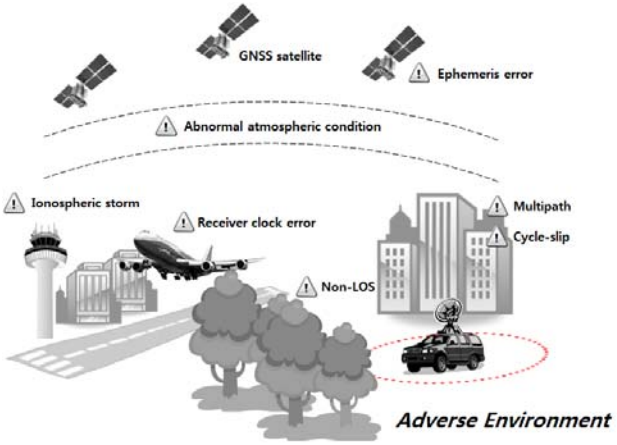

Fig. 1 Various error sources in GNSS

II. Adaptive Detection Method

The proposed adaptive detection method consists of two parts; measurement noise covariance estimation and adaptive fault detection. During the noise covariance estimation, pseudorange and carrier-phase measurement noise covariances are estimated based on Innovation-Based Adaptive Estimation (IAE) method [8], [9]. By the CSC filtering, the pseudorange and carrier-phase innovation sequences are obtained at time propagations and measurement updates, respectively. Based on these innovations, noise covariances can be estimated. During the adaptive fault detection, abnormal trends in the measurement errors for each channel are checked for detecting fluctuating or slowly varying soft faults independent of

This research was supported by a grant from National Agenda Project (NAP) funded by Korea Research Council of Fundamental Science & Technology.

J. Y. Lee, H. S. Kim, K. H. Choi, and J. H. Lim are with the School of Electronics and Telecomm., Korea Aerospace University, Korea (e-mail: jeylee@kau.ac.kr, hskim07@kau.ac.kr, sahnhara@kau.ac.kr, limjh@kau.ac.kr).

S. B. Chun is with the Korea Aerospace Research Institute, Korea (e-mail: sbchun@kari.re.kr).

H. K. Lee was with Hyundai Space and Aircraft Corporation, Korea. He is now with the School of Electronics and Telecomm at Korea Aerospace University, Korea, as an Associate Professor (corresponding author to provide phone: 82-2-300-0131; fax: 82-2-3159-9257; e-mail: hyknlee@kau.ac.kr).

satellite-receiver geometries and filter estimates. To generate test statistics for fault detection, the previously estimated measurement noise covariances are utilized. This combined procedure enables effective fault detection considering various time-varying environments of the receiver.

A. Measurement Noise Estimation

In CSC filtering, carrier-phase measurements are utilized to generate a priori state estimates at time propagation. The innovation sequence of carrier-phase measurements can be obtained the difference between the actual measurement and its estimates.

$$Z_{\Phi,k} = \Omega_{k+1} - H_{k+1}\Delta\hat{X}_k \tag{1}$$

In (1), Ω_{k+1} indicates the indirect measurement, H_{k+1} indicates the observation matrix, $\Delta\hat{X}_k$ indicates *a posteriori* state estimates and the subscript Φ indicates carrier-phase measurement. By the singular value decomposition [10], the carrier-phase measurement noise can be obtained following equations.

$$\hat{\sigma}^2_{\Phi,k} = \frac{1}{n}\sum_{i=1}^{n} diag(M_{k,i}) \tag{2}$$

where,

$$M_k = \left(V\Sigma'\right)^{-1} E\left\{Z_{\Phi,k}Z_{\Phi,k}{}^T\right\}\left(\Sigma'^T V^T\right)^{-1} \tag{3}$$

$$U\Sigma V^* = \left(I - H_{k+1}H^+_{k+1}\right)\left(I - H_{k+1}H^+_{k+1}\right)^T \tag{4}$$

$$H^+_k = \left(H^T_k H_k\right)^{-1} H^T_{k+1} \tag{5}$$

$$\Sigma' = \Sigma^{\frac{1}{2}} \tag{6}$$

Similar to the case of carrier-phase measurements, the pseudorange measurement noise can be estimated based on innovations at measurement update. The innovation sequence of pseudorange measurements is modelled by

$$Z_{\rho,k} = H_k\bar{X}_k - Y_k \tag{7}$$

In (7), Y_k indicates the actual measurement, $\bar{X}_k$ indicates *a priori* state estimates and the subscript ρ indicates pseudorange measurement. The pseudorange measurement noise can be obtained following equations.

$$\hat{R}_{\rho,k} = C_{\rho,k} - H_k\bar{P}_k H^T_k \tag{8}$$

where,

$$C_{\rho,k} = E\left\{Z_{\rho,k}Z^T_{\rho,k}\right\} \tag{9}$$

$$\hat{R}_{\rho,k} = \begin{bmatrix} \hat{\sigma}^2_{\rho,1} + \hat{\sigma}^2_{\rho,r} & \hat{\sigma}^2_{\rho,r} & \cdots & \hat{\sigma}^2_{\rho,r} \\ \hat{\sigma}^2_{\rho,r} & \hat{\sigma}^2_{\rho,2} + \hat{\sigma}^2_{\rho,r} & & \vdots \\ \vdots & & \ddots & \hat{\sigma}^2_{\rho,r} \\ \hat{\sigma}^2_{\rho,r} & \cdots & \hat{\sigma}^2_{\rho,r} & \hat{\sigma}^2_{\rho,n-1} + \hat{\sigma}^2_{\rho,r} \end{bmatrix} \tag{10}$$

In (8), $\bar{P}_k$ indicates the *a priori* error covariance matrix and $\hat{\sigma}^2$ indicates the estimated noise variance. As shown in (2) and (10), in the case of carrier-phase measurement, a common deviation is computed. However, in the case of pseudorange, deviations are computed channel-by-channel. It is because the carrier-phase measurements show similar error characteristics and pseudorange measurements show quite different error characteristics between different channels, which is mainly caused by different sensitivities to multipath errors. Thus it can be assumed that the carrier-phase variance originating from different channels are the same and not correlated to each other.

B. Adaptive Fault Detection

The adaptive fault detection method checks abnormal trends in the variance of pseudorange and carrier phase measurement sequence based on the estimated measurement noise. The projected pseudorange vector is modelled by

$$\begin{aligned} S^j_k = [\ & \tilde{\rho}^j_{k-1} + \left(\tilde{\Phi}^j_k - \tilde{\Phi}^j_{k-1}\right) \quad \tilde{\rho}^j_{k-2} + \left(\tilde{\Phi}^j_k - \tilde{\Phi}^j_{k-2}\right) \\ & \cdots \quad \tilde{\rho}^j_{k-B} + \left(\tilde{\Phi}^j_k - \tilde{\Phi}^j_{k-B}\right)\ ]^T \end{aligned} \tag{11}$$

The projected residual vector can be obtained by the difference between the projected pseudorange vector and the actual pseudorange measurements.

$$D^j_k = \rho^j_k \cdot l - S^j_k \tag{12}$$

In (12), l denotes the vector whose elements are all set to 1 for the expansion from a scalar value to a vector. Based on the projected residual vector, the test statistics for fault detection is modelled by

$$TS^j_{RD} = \frac{1}{\sigma^2_{RD}} Z^T_{RD} K^T \left(KK^T\right)^{-1} KZ_{RD} \tag{13}$$

where,

$$\sigma^2_{RD} = \sigma^2_\rho + \sigma^2_\Phi + \sigma^2_{others} \tag{14}$$

$$Z_{RD} = \begin{bmatrix} \rho^j_k - \Phi^j_k \\ \rho^j_{k-1} - \Phi^j_{k-1} \\ \vdots \\ \rho^j_{k-B} - \Phi^j_{k-B} \end{bmatrix} \tag{15}$$

$$K = \begin{bmatrix} 1 & -1 & \cdots & & 0 \\ 1 & 0 & -1 & & \vdots \\ \vdots & & \ddots & \ddots & \\ 1 & \cdots & 0 & 0 & -1 \end{bmatrix} \tag{16}$$

As shown in (14), the noise variance of test statistics is

composed of the carrier-phase and pseudorange measurement noise variances. Thus, (14) can be replaced utilizing (2) and (10) as follows.

$$\hat{\sigma}_{RD}^2 = \hat{\sigma}_{\rho}^2 + \hat{\sigma}_{\Phi}^2 \tag{17}$$

In (17), it is assumed that σ_{others}^2 is small enough to be ignored as compared with the carrier-phase and pseudorange measurement noise variances. By utilizing the noise variances estimated in real-time, effective fault detection considering receiver's operating environment is enabled.

III. Experimental Results

Performance of the proposed adaptive fault detection method was evaluated by an experiment. For the experiment, two GPS receivers were utilized to collect actual GNSS measurements. A NovAtel DL-V3 receiver mounted on a vehicle was utilized as the rover and a Septentrio PolaRX2e receiver was utilized as the reference. All the raw measurements of the reference and rover receivers were logged in the standard receiver independent exchange (RINEX) format. Both receivers provide dual-frequency measurements. However, only single-frequency measurements were utilized to evaluate the performance. The field-collected dual-frequency measurements were processed to extract reference trajectory based on integer ambiguity resolution. The experiment was performed near Korea Aerospace University.

To evaluate fault detection capability of the proposed method, intentional faults of abrupt jumps were added to field collected measurements. Fig. 2 shows the injected fault profile. The intentional faults were added to PRN 8, 19 satellites with 10 meter magnitudes and to PRN 6, 11 satellites with 15 meter magnitudes.

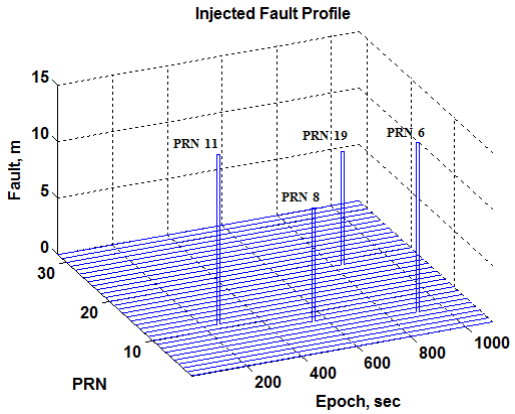

Fig. 2 Injected intentional fault profile

Figs. 3 and 4 show the estimated standard deviations of carrier-phase and pseudorange measurements, respectively. The standard deviation is the square-root of the variance. As explained above, in the case of pseudorange measurement, standard deviations were computed channel-by-channel. However, in the case of carrier-phase measurements, a common standard deviation was computed since their errors are far less sensitive to signal environments than pseudorange measurement errors.

Figs. 5 and 6 show the adaptive test statistics for fault detection generated by the proposed adaptive method under normal conditions and simultaneous abrupt jumps are added, respectively. Since each abrupt jump can be detected clearly as shown in Fig. 6 by the proposed adaptive detection method, the unhealthy measurement can be effectively isolated in positioning.

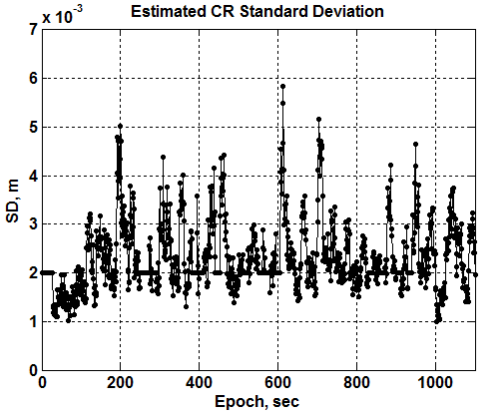

Fig. 3 Estimated carrier-phase standard deviations

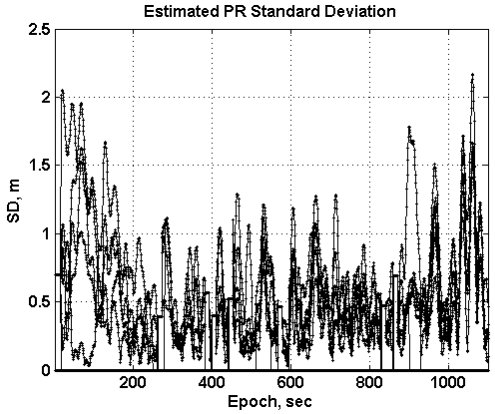

Fig. 4 Estimated pseudorange standard deviations

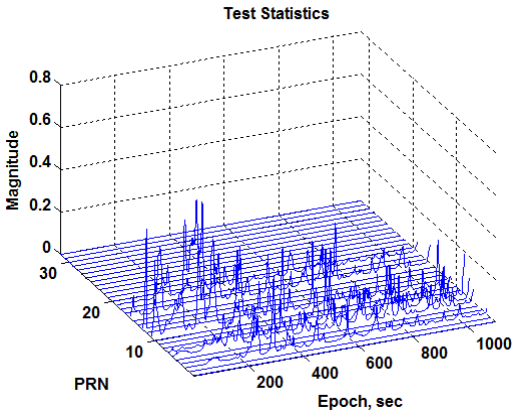

Fig. 5 Adaptive test statistics without fault injection

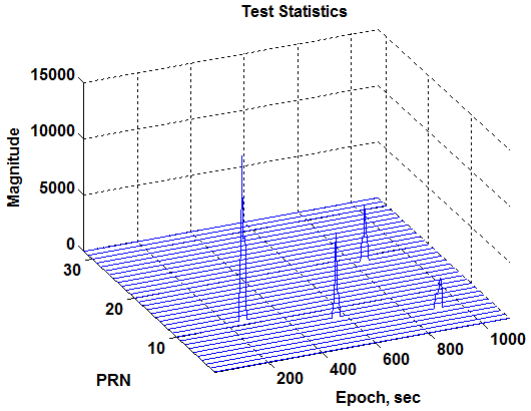

Fig. 6 Adaptive test statistics with fault injection

Fig. 7 shows the experimental trajectory of the rover vehicle. In Fig. 7, the black circles correspond to CSC filter with the proposed adaptive detection method and the grey circles correspond to the CSC filters without detection method. Due to the large scale of the figure, the two different trajectories cannot be discriminated.

Figs. 8 and 9 show error magnitudes by comparing the estimated and reference trajectories in both horizontal and vertical directions for more detailed evaluation. Figs. 8 and 9 show the horizontal and vertical errors, respectively. As shown in the figures, the positioning accuracy improves remarkably mainly by the fault detection capability under fault occurrences.

IV. Conclusion

In this paper, an efficient adaptive fault detection method was proposed for GNSS applications. The proposed method utilizes the adaptive test statistics for fault detection based on the measurement noise variances estimated in real-time. The measurement noise variances are estimated by the modified CSC filtering. The performance of the proposed method was evaluated by a field experiment. By the experimental result, it was confirmed that the proposed method shows the capability of detecting and identifying faults and improves positioning accuracy by adaptive test statistics.

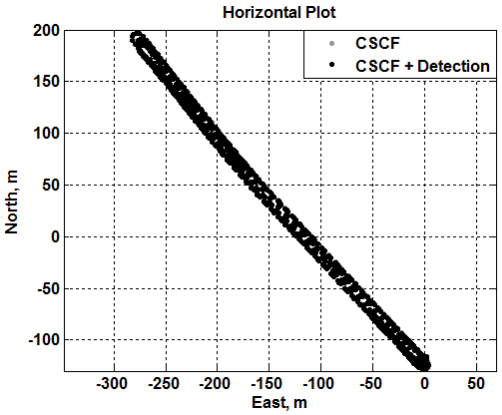

Fig. 7 Comparison of trajectories

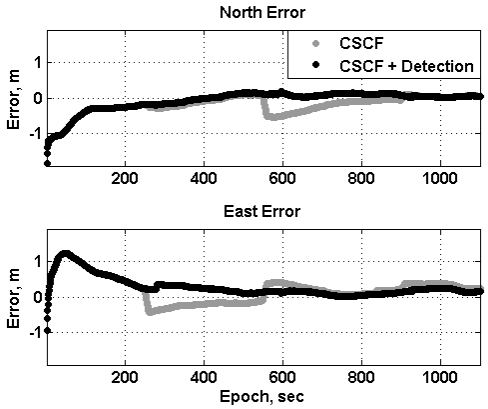

Fig. 8 Comparison of error magnitudes in horizontal direction

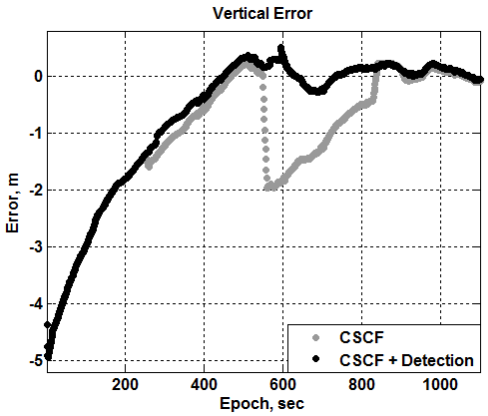

Fig. 9 Comparison of error magnitudes in vertical direction

References

[1] S. Hewitson, J. Wang, "GNSS receiver autonomous integrity monitoring (RAIM) performance analysis," *GPS Solutions*, 10(3), 2006, pp. 155-170.

[2] Y. C. Lee, "A position domain relative RAIM method," *Aerospace and Electronic Systems, IEEE Transactions on*, 47(1), 2011, pp. 85-97.

[3] J.Wang, P. B. Ober, "On the availability of fault detection and exclusion in GNSS receiver autonomous integrity monitoring," *Journal of Navigation*, 62(02), 2009, pp. 251-261.

[4] M. A. Sturza, "Skewed axis inertial sensor geometry for optimal performance," In *8th AIAA/IEEE Digital Avionics Systems Conference*, Vol. 1, 1988, pp. 128-135.

[5] E. D. Kaplan, and C. J. Hegarty, (Eds.), *Understanding GPS: principles and applications*. Artech house, 2005.

[6] J. Y. Lee, H. S. Kim, H. K. Lee, "Detection of multiple faults in single-frequency differential GPS measurements," *IET Radar, Sonar & Navigation*, 6(8), 2012, pp. 697-707.

[7] R. Hatch, "The synergism of GPS code and carrier measurements," In *International geodetic symposium on satellite doppler positioning*, Vol. 1, 1983, pp. 1213-1231.

[8] R. K. Mehra, "On the identification of variances and adaptive Kalman filtering," *Automatic Control, IEEE Transactions on*, 15(2), 1970, pp. 175-184.

[9] R. K. Mehra, "On-line identification of linear dynamic systems with applications to Kalman filtering," *Automatic Control, IEEE Transactions on*, 16(1), 1971, pp. 12-21.

[10] G. H. Golub, C. Reinsch, "Singular value decomposition and least squares solutions," *Numerische Mathematik*, 14(5), 1970, pp. 403-420.